INTERFEROMETER OBSERVATIONS OF A RADIO BURST AT 8.6 mm ASSOCIATED WITH A POLARIZED HARD X-RAY EVENT

K. KAWABATA, Y. SOFUE, H. OGAWA, and T. OMODAKA
Dept. of Physics, Nagoya University, Nagoya, Japan

(Received 20 November, 1972; in revised form 6 June, 1973)

Abstract. Observations of a radio burst at 8.6 mm wavelength on 1970 November 5, are described with the particular interest on the correspondence between radio and polarized X-ray events. The radio observations were carried out using an interferometer with a half power width of 2.9′ at the Dept. of Physics, Nagoya University, and indicated that the location of the radio burst coincided with preceding sunspots and the size of the burst source must be very small, less than about 1′. Mechanisms of radio and X-ray emissions are discussed briefly.

1. Introduction

A two-ribbon flare of importance 3B (private communication from the Tokyo Astronomical Observatory) occurred on 1970 November 5 at S12/E37 in a plage region McMath No. 11019 (see *Solar-Geophysical Data* issued by U.S. Dept. of Commerce, National Oceanic and Atmospheric Administration, Environmental Data Service). Observations of the associated radio burst at 8.6 mm wavelength were carried out at the Dept. of Physics, Nagoya University, using a four element east-west interferometer (Figure 1). The instrument has a half-power beam width of about 2.9′ and a beam separation of about 12.6′ near the meridian plane. The time interval between observations due to drift scanning depends on the declination and on the observing time, and is about 50 s at the meridian transit. The performance of the instrument is described in more detail elsewhere (Kawabata and Sofue, 1972).

The solar event on 1970 November 5 is of particular interest in that we have radio data on the location and the size of the radio burst at 8.6 mm from the interferometer, linear polarization data on the hard X-ray event from Intercosmos-4 satellite (Tindo *et al.*, 1972a), and a lot of other observational data. In the present article, we describe briefly the 8.6 mm observations with the particular interest on the detailed correspondence between radio and X-ray events, and we discuss the physical implications of the observations in order to throw some light on the solar mechanism involved.

2. Observations

The two-ribbon flare on 1970 November 5 started at 0308 UT and attained full development at 0323. The sunspots associated with the active region, in which the flare occurred, were not so large but had strong magnetic fields of up to 2500 G (Academy

Solar Physics **31** (1973) 469–481.

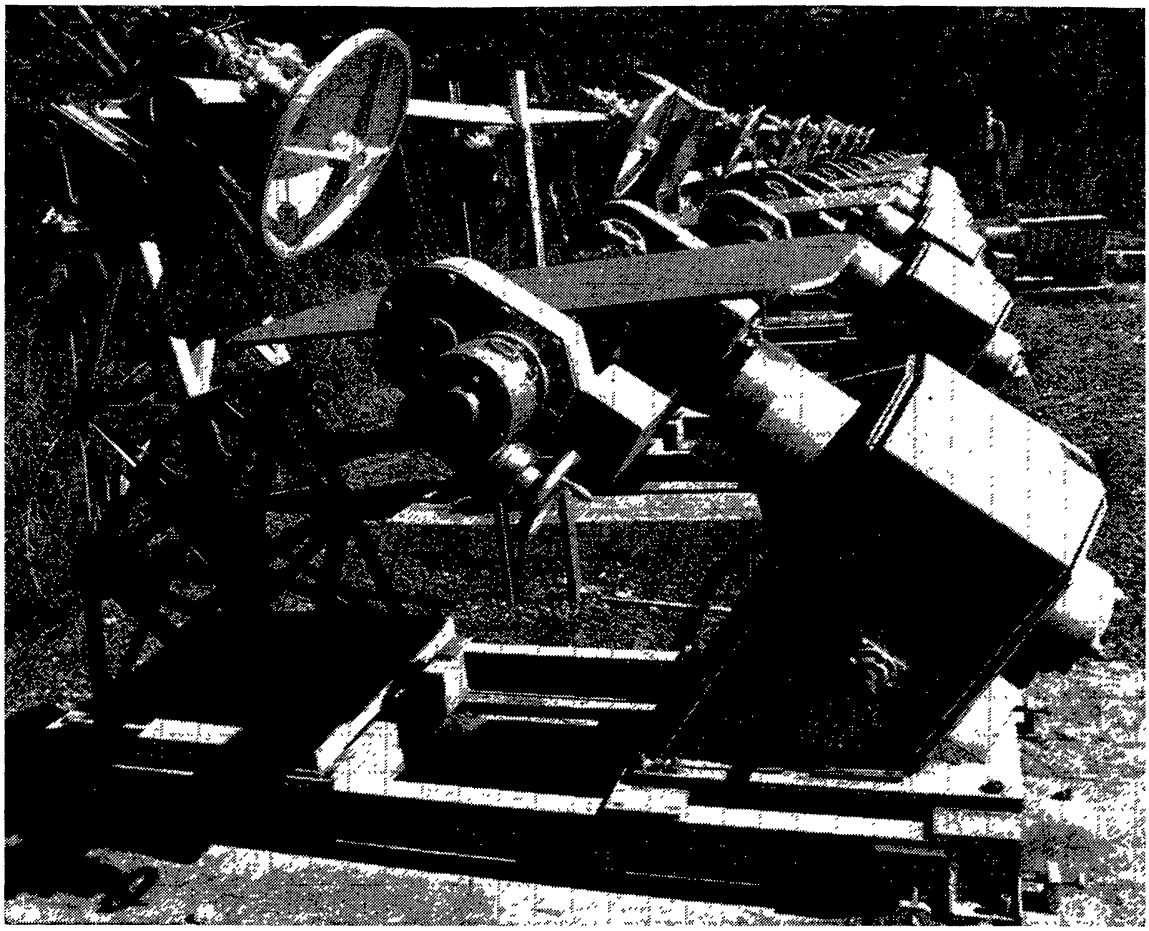

Fig. 1. The 8.6 mm interferometer at the Dept. of Physics Nagoya University. The instrument has been extended to an eight element interferometer with a half power beam width of 1.5′.

of Science, U.S.S.R., 1970). The associated hard X-ray event observed by Tindo *et al.* (1972a) started at 0316 UT and consisted of two successive bursts peaking at 0320 and 0329, respectively. The degree of polarization of the X-ray event attained a maximum value as high as 21% at the time of maximum intensity of the first X-ray burst. However, the observations did not show any indication of a peak in the degree of polarization at the time of maximum intensity of the second X-ray burst. The polarization degree of the second X-ray burst was less than 10%.

Figure 2 gives a comparison of our radio observations with the hard X-ray observations by Tindo *et al.* (1972a). The radio flux density at 8.6 mm started to increase gradually in coincidence with the starting time of the X-ray event, but the flux density at 8.6 mm remained small until about 0325. At about 0325 UT, the 8.6 mm flux density increased abruptly and attained a value of 260 f.u. (10^{-22} W m^{-2} Hz^{-1}) at 0326. The time of peak flux density at 8.6 mm approximately coincided with that of the second X-ray burst. The 8.6 mm observation did not show any indication of a peak at the time of maximum intensity of the first X-ray burst. The correspondence between 8.6 mm and hard X-ray bursts appears to indicate that an X-ray burst with a large degree of polarization is associated with only a small increase in the 8.6 mm emis-

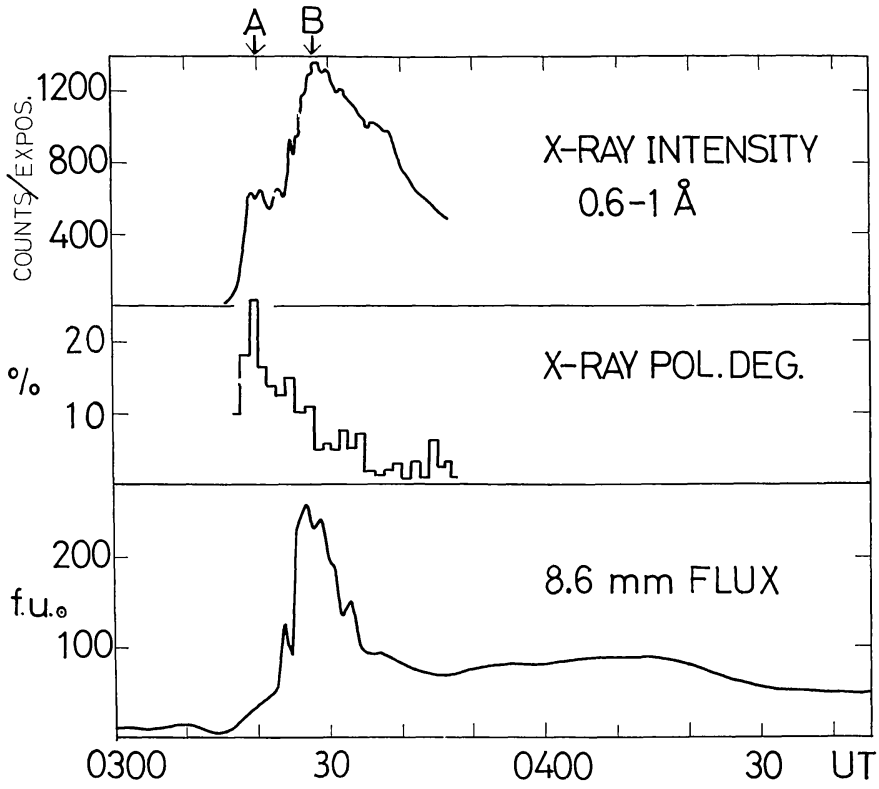

Fig. 2. A comparison of 8.6 mm flux density (in 10^{-22} Wm^{-2} Hz^{-1}) with an intensity (in counts/expos.) and a degree of polarization of X-rays observed by Tindo *et al.* (1972a).

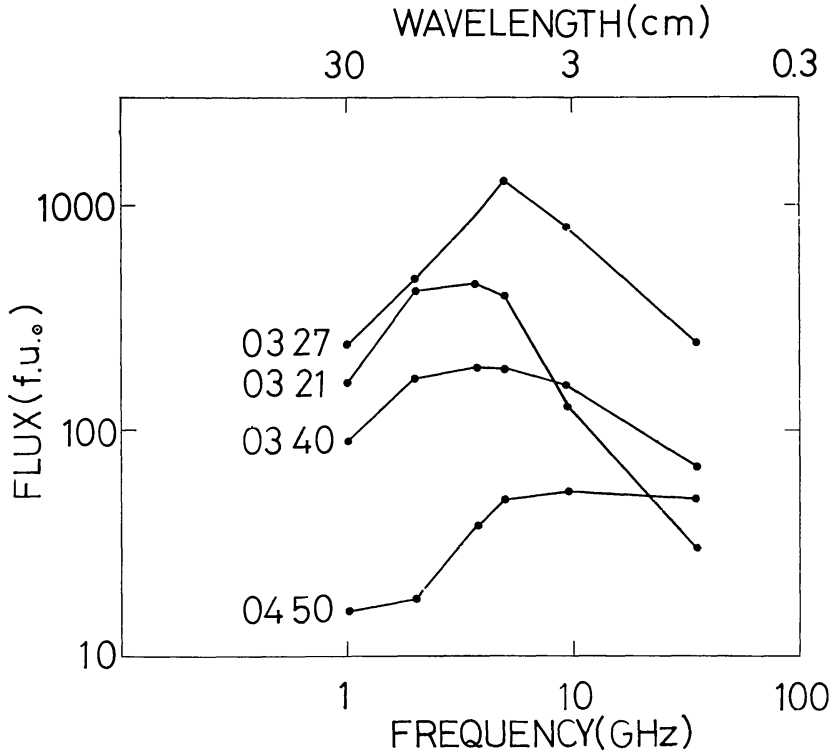

Fig. 3. Radio spectra at the time of the first X-ray burst (0321 UT), the impulsive phase of the 8.6 mm burst (0327 UT), the early period of the post-burst increase (0340 UT), and the late period of the post-burst increase (0450 UT).

sion, if any, and an X-ray burst with small degree of polarization is associated with a large increase in the 8.6 mm emission. The impulsive phase of the 8.6 mm burst ended at about 0334 UT before the end of the hard X-ray burst, and it was followed by a post-burst increase with a flux density of 90 f.u., lasting more than 100 min.

Figure 3 illustrates radio spectra at the impulsive and post-burst phases of the radio burst. The radio data longer than λ 3 cm were kindly made available by Prof. H. Tanaka, Research Institute of Atmospherics, Nagoya University. During the impulsive phase, the radio spectrum had a maximum flux density at about λ 5 cm and showed a steep decrease of flux density towards shorter wavelength below the maximum. During the post-burst phase, the spectrum became broadened as time elapsed, and finally became flat at wavelengths shorter than 8 cm. Such a change of spectrum has been already pointed out by Feix (1968) as a general feature of the post-burst phase.

Figure 4 gives a comparison between our radio data from drift scannings and a sketch of sunspots. The sketch of sunspots was kindly made available by Prof. F. Moriyama, Tokyo Astronomical Observatory, University of Tokyo. The magnetic field strengths observed at the Crimean Astrophysical Observatory (Academy of Science, U.S.S.R., 1970) are also shown in the figure. Note that before 0325 UT, the 8.6 mm emission was either only slightly greater than our observational errors or

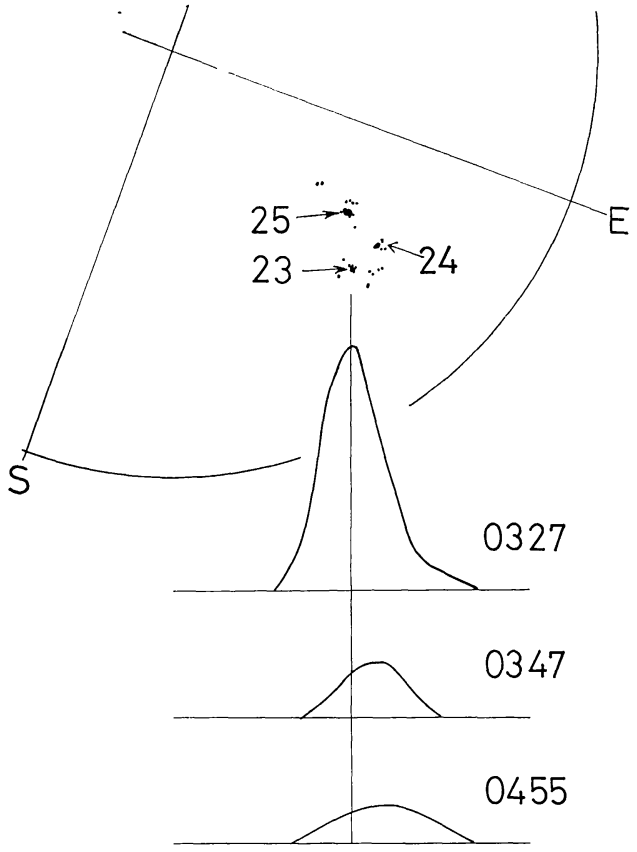

Fig. 4. A comparison between observed brightness distributions at 8.6 mm and a sketch of sunspots. Magnetic field strengths of sunspots in unit of 100 G (Academy of Science U.S.S.R., 1970) are also indicated.

else it was increasing rapidly, hence deforming the scanning curve, and in both these cases the precise location and size of the 8.6 mm emission region is questionable.

During the impulsive phase from 0325 through 0331, two preceding sunspots with strong magnetic fields, 2500 and 2300 G respectively, were located on the line of possible location of the radio burst source. The observed half power width of the drift scanning was about 3.0′. Since the observed half power width was very close to the theoretical half power beam width of 2.9′, the source size must be very small. If we assume that the one-dimensional brightness distribution of the 8.6 mm burst is Gaussian, then the half power width of the source becomes less than about 1′.

After 0331 UT, the location of the radio emission at 8.6 mm shifted east-wards from the preceding sunspots. The location of the center of 8.6 mm emissions coincided with the center of the active region rather than with the preceding sunspots during the post-burst phase. The observed half power width was 3.5–4.0′ in this period. Since the observed half power width during the impulsive phase was very close to the theoretical half power beam width, the broadening was probably not due to the instrumental errors but probably real. If we again assume a Gaussian distribution for the brightness, then the observed half power width corresponds to a half power width of the brightness as wise as about 2.5′.

3. Interpretation of Results by the 'Thick Target Model'

It is now generally accepted that hard X-ray and microwave bursts are generated by high energy electrons with a common origin. Anderson and Winckler (1962) proposed the 'thick target model', in which these electrons are accelerated in the coronal region and impinge on the chromosphere continuously throughout a burst. Elwert and Haug (1970) predicted linear polarization of the X-rays by assuming that X-ray bursts are produced by highly directed electron beams. The discovery of the linear polarization of X-rays by Tindo *et al.* (1970) appears to confirm the model. Since the mean free path of 10 keV electrons is 10^{10} cm in the corona with an electron density of 3×10^{9} cm^{-3}, electrons with energy exceeding 10 keV are spiralling around a magnetic line of force. Now we suppose that these electrons are accelerated nearly parallel to the magnetic field in a region of the corona with a weak magnetic field, presumably close to the neutral sheet of the active region, and impinge on the chromosphere through a magnetic flux tube with a cross section $A(f_H)=A_0 f_{H_0}/f_H$. Here f_H denotes the local electron gyro-frequency and the suffix '0' indicates the value at the field strength H_0. We assume that the number of electrons with energy between E and $E+\mathrm{d}E$ per unit volume and per unit solid angle is given by

$$\mathrm{d}N' \begin{cases} = (\delta-1)\,N\,(E/E_1)^{-\delta}\,\mathrm{d}\,(E/E_1) & \text{for} \quad E_1 \leqslant E \leqslant E_2 \\ = 0 \quad \text{for} \quad E < E_1 \quad \text{and for} \quad E_2 < E \end{cases} \tag{1}$$

in a cone with an apex angle ψ from the direction of the magnetic field and is zero outside this cone. Because of the absence of collisions, the following relations are

satisfied throughout the magnetic flux tube,

$$\frac{\sin^2\psi}{f_H} = \frac{\sin^2\psi_0}{f_{H_0}} \quad \text{and} \quad N = \text{const.} \tag{2}$$

The emissivity of the gyro-resonance emissions per unit volume at a frequency f per unit frequency range is given by

$$\eta_f = \frac{(2\pi)^2 e^2 f^2}{c} \sum_{s=1}^{\infty} \frac{s^{2s}}{2^{2s}(s!)^2} \iint (1+\cos^2\theta) \sin^{2s-2}\theta \sin^{2s+1}\varphi \times$$
$$\times \left(\frac{2E}{mc^2}\right)^s \delta(f - sf_H)\, \mathrm{d}N'\, \mathrm{d}\varphi, \tag{3}$$

in the non-relativistic approximation by neglecting the Doppler shift (see for instance, Bekefi, 1966). Here θ and φ denote respectively the angle between the line of sight and the magnetic field and the angle between the electron velocity and the magnetic field. Unspecified symbols have their usual meaning.

In deriving Equation (3), the Bessel functions in the exact formula are replaced by their first terms of the series expansions for small arguments. Such an approximation may produce an overestimation in the integrand of the formula on the emissivity by a factor of 3 at $\beta = 0.55$ (100 keV). The emissivity given by Equation (3) is in closer proximity to the exact value than the above estimation, because the approximation is better for the most of electrons. Since we are intending to deal with only the order of magnitude of radio emissions, the approximation will be sufficient for the present purpose. A replacement of β by $(2E/mc^2)^{1/2}$ does not give the exact value of β. The approximation, however, is equivalent to some modification of electron spectrum from Equation (1) close to the high energy cut-off. Since the high energy cut-off of the electron spectrum is introduced arbitralily to some extent, such a modification of the electron spetrum is of no physical importance.

Integrating Equation (3) over the whole magnetic flux tube in which these electrons are flowing downwards, one obtains the flux density at the Earth heliocentric distance R at the frequency f

$$S_f = \frac{(2\pi)^2 e^2 f^2}{R^2 c} (\delta - 1) N \sum_{s=n}^{\infty} \frac{s^{2s}}{2^{2s}(s!)^2} \int A(f_H)\, \delta(f - sf_H)\, (1+\cos\theta^2) \times$$
$$\times \sin^{2s-2}\theta\, \mathrm{d}l \int_1^{E_2/E_1} \left(\frac{E}{mc^2}\right)^s \left(\frac{E}{E_1}\right)^{-\delta} \int_0^{\psi(f_H)} \sin^{2s+1}\varphi\, \mathrm{d}\varphi, \tag{4}$$

after simple manipulation. Here $\mathrm{d}l$ denotes the line element along the magnetic line of force. Gyro-resonance radiation is emitted at the same frequency f from various cross sections of the magnetic flux tube at discrete heights due to the various harmonics of the local gyro-frequency. Each term of summation in Equation (4) corre-

sponds to emission from each cross section and the first term, $s=n$, corresponds to emission from the lowest one. The value of n depends on the frequency and on the field strength of the chromosphere where the electron beam impinges.

Since the magnetic field strength varies along the magnetic flux tube in the present model, $\mathrm{d}l$ in Equation (4) relates to $\mathrm{d}f_H$ in the following form

$$\mathrm{d}l = L(f_H)\,\mathrm{d}f_H/f_H\,. \tag{5}$$

Here $L(f_H)$ denotes the characteristic variation length of the magnetic field, i.e., $L(f_H)=f/(\mathrm{d}f_H/\mathrm{d}l)$.

By inserting Equation (5) and $A(f_H)f_H=A_0 f_{H_0}$ into (4), one obtains

$$\begin{aligned} S_f = {} & \frac{(2\pi)^2 e^2}{R^2 c}(\delta-1)\,A_0 L_0 N f_{H_0} \sum_{s=n} \frac{s^{2s+1}}{2^{2s}(s!)^2}(1+\cos^2\theta)\sin^{2s-2}\theta \times \\ & \times \frac{L(f/s)}{L_0}\left(\frac{2E_1}{mc^2}\right)^s \int_0^{\psi(f/s)} \sin^{2s+1}\varphi\,\mathrm{d}\varphi \times \\ & \times \begin{cases} \dfrac{1}{n-\delta+1}\left\{\left(\dfrac{E_2}{E_1}\right)^{n-\delta+1}-1\right\} & \text{for} \quad n-\delta+1\neq 0 \\ \ln\dfrac{E_2}{E_1} & \text{for} \quad n-\delta+1=0 \end{cases} \end{aligned} \tag{6}$$

after integration on f_H and E. Here $L_0=L(f_{H_0})$. $L(f/s)/L_0$ is close to unity and varies slowly compared with the other factors. In the following, we assume $L(f/s)/L_0=1$ and only the first term of the summation in Equation (6) is retained. We take the field strength at the height of 8.6 mm emission as H_0.

Now we apply Equations (2) and (6) to the present event for a study on relations between hard X-ray and radio bursts. Observations of X-rays by Tindo *et al.* (1972b) shows that the present event has an integrated X-ray spectrum proportional to $(h\nu)^{-3}$ above $h\nu=10$ keV. The X-ray spectrum indicates $\delta=5.5$, if we adopt the thick target model. Since the X-ray spectrum obtained by Tindo *et al.* (1972b) is curved below 10 keV, we adopt $E_1=10$ keV. We assume that $E_2=100$ keV, since Kane and Anderson (1970) showed that the X-ray spectra has a sharp cutoff at about 100 keV.

Zheleznyakov (1962) showed that at the height of the second harmonic the thermal electrons are opaque due to gyro-resonance absorption at about 3 cm wavelength. Therefore the radio emission at 3.2 cm will be emitted mainly at the height of the third harmonic. Then we assume $n=3$ at $\lambda=3.2$ cm. Figure 5 shows the ratio of the flux densities at 8.6 mm and 3.2 cm calculated using Equations (2) and (4) for various values of n at 8.6 mm.

Figure 5 indicates that $n\geqslant 7$ at 8.6 mm can not give the observed ratio of 0.3, assuming that the characteristic variation length of the magnetic field is not so different between the corresponding two emission layers. This means that the electrons are impinging on the chromosphere with a magnetic field exceeding 2000 G. Since the

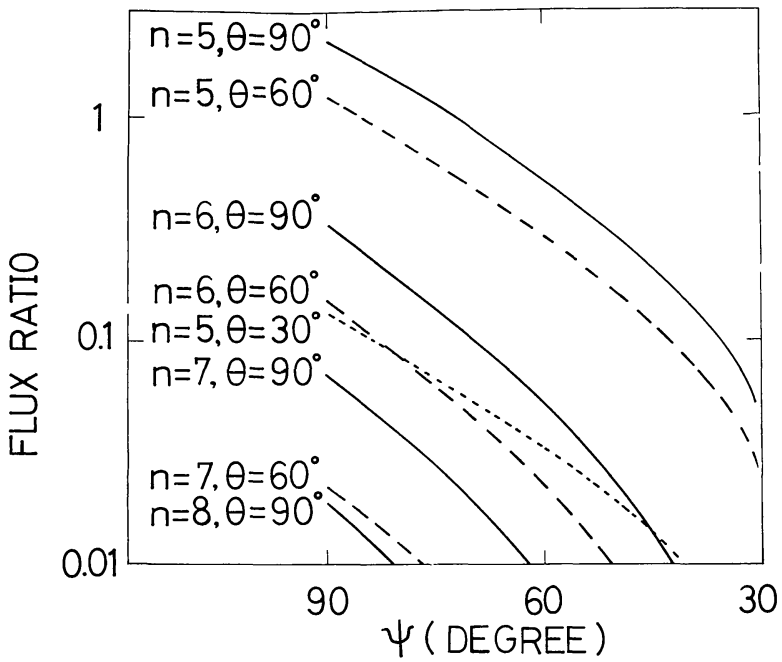

Fig. 5. Ratio of flux densities $S_{8.6\,\mathrm{mm}}/S_{3.2\,\mathrm{cm}}$. n is the harmonic number of the gyro-resonance emission at 8.6 mm. θ denotes the angle between the magnetic field and the line of sight.

highest field strength of sunspots was 2500 G, n must be equal to or larger than 5 at 8.6 mm. In this case, the radio spectrum between 3.2 cm and 8.6 mm can be accounted for only if the angle between the line of sight and the magnetic field is more than about 60°, and the apex angle of the velocity cone of the electron beam is more than 50°. Table I summarizes the parameters in the thick target model which are able to account for the flux density at 8.6 mm and 3.2 cm.

Now, we evaluate the emission measure (E.M.) given by Equation (A-5) from the radio parameters for a comparison with X-ray data. Since the required field strength at the height of 8.6 mm emission is close to the highest field strength in the photosphere, ψ and $A(f_H)$ at the chromospheric height will be close to those at the height

TABLE I

Parameters on an electron beam producing an 8.6 mm burst

	Radio model			X-ray observation
H_0 (gauss)	2500	2500	2100	
n at 8.6 mm	5	5	6	
θ (deg)	90	60	90	
ψ_0 at 8.6 mm (deg)	50	61	88	
ψ at 3.2 cm (deg)	31	36	47	
$2\pi A_0 L_0 N(1-\cos\psi_0)$, 0321 UT ($10^{35}$ electrons)	1.9	1.3	0.29	
$2\pi A_0 L_0 N(1-\cos\psi_0)$, 0327 UT ($10^{35}$ electrons)	0.22	0.15	0.034	
E.M., 0321 UT (10^{45} cm^{-3})	0.32	0.23	0.05	16
E.M., 0327 UT (10^{45} cm^{-3})	2.8	2.0	0.43	30

of 8.6 mm emission. Then we assume ψ_c and A_c in Equation (A-5) (the suffix c indicates the value at the chromospheric height) are equal to ψ_0 and A_0, respectively. We also assume $L_0 = 3 \times 10^9$ cm. The emission measures evaluated in this way are also tabulated in Table I.

From an X-ray observation, we estimate the emission measure using Equation (A-7). The X-ray observation by Tindo *et al.* (1972b) gives an emission measure of 1.6×10^{46} cm^{-3} for the first X-ray burst. If we assume the same X-ray spectrum for the second X-ray burst as that for the first burst, the emission measure for the second burst becomes 3×10^{46} cm^{-3}. The emission measure for X-ray observations was more than ten times larger than the emission measure for radio observations.

At about 3 cm, the optical depth of the layer of the third harmonic may become approximately unity for the extraordinary mode due to gyro-resonance absorption by thermal electrons. Since the gyro-resonance emission is mainly emitted in the extraordinary mode, the radio flux densities at 3.2 cm will be overestimated by a factor of 3. Note that the third harmonic of the gyro-resonance emission due to the electron beam is emitted just below the thermal electron absorbing layer because of the redshift in the emission. Even if we take into account the absorption in the layer of the third harmonic, the conclusions about the apex angle of the electron beam and the angle between the line of sight and the magnetic field will not be changed because these angles are only weakly dependent on the ratio of the flux densities.

In this case, however, the calculated emission measure in the table will be underestimated by a factor of 10 due to the strong dependence of the flux density on the angles. This might to a certain extent account for the discrepancies between the observed and calculated values of E.M., however it seems difficult to explain the difference in the relative time variations in this way.

4. Discussions and Conclusions

At the time of the first X-ray burst (stage A), the X-ray intensity reached about half of that at the time of the radio peak (stage B), but the radio flux density was only a tenth of that at the peak flux density. At stage A, most of high energy electrons are dumped in the weak field region and only a small number of the electrons impinge on the strong field region. The observation of X-ray polarization indicates that the former electrons are highly directed. The radio spectrum between 3.2 cm and 8.6 mm suggests that the latter electrons had a large apex angle and impinge on the chromosphere with a magnetic field exceeding 2100 G. The apex angle of the electron beam at the chromosphere is connected with the field strength of the chromosphere where these electrons impinge.

During the impulsive phase of the 8.6 mm emission (stage B), the coincidence of the location of radio source with that of the sunspots and the small size of radio source suggest that a number of electrons impinge on sunspot which has a magnetic field of 2500 G or 2300 G or both. The radio spectrum between 3.2 cm and 8.6 mm is consistent with this conclusion. The radio spectrum also suggests that the electron beam

has a broad directivity. The degree of polarization of X-rays was smaller in stage A than in stage B. The decrease of the degree of X-ray polarization is connected with the increase of the number of electrons impinged on sunspot region.

Figure 6 shows two field configurations which would produce such a change in the electron beam. The field configuration in Figure 6a does not change with time, but the electron beam moves from A to B. While in Figure 6b, the reconnection of the magnetic field occurs at the *Y*-shaped neutral line and the field configuration changes from A to B as time elapses.

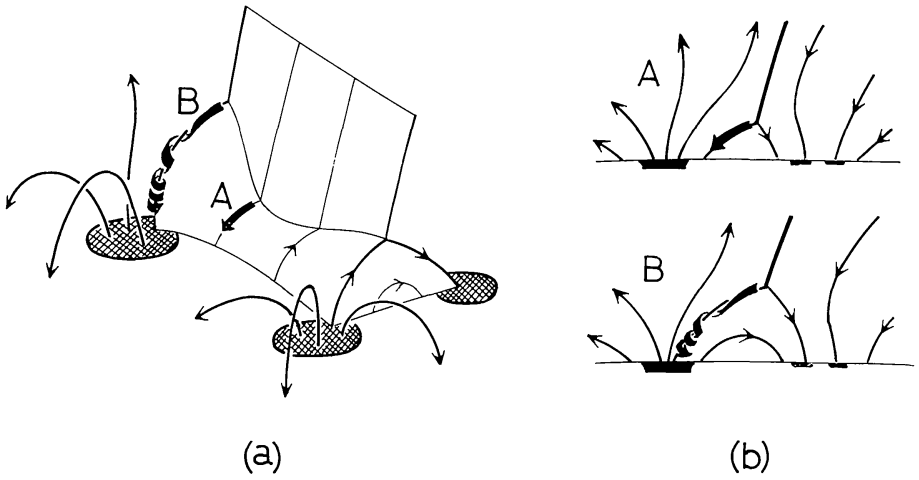

Fig. 6. Magnetic field configuration and the location of the electron beam. (a) Magnetic field configuration does not change with time. The most of electrons are streaming downwards at A during the first X-ray burst, and the large number of electrons are streaming at B during the impulsive phase of 8.6 mm burst. (b) reconnection of the magnetic field occurs on the *Y*-shaped neutral line, and the location of the electron beam moves from A to B.

The emission mechanism of post burst increases was confirmed to be free-free emission from a high temperature, optically thin plasma, by Feix (1968) and Hudson and Ohki (1972) from observations at 8.5 mm and 1.8 cm. The flat spectrum at the late stage of the post-burst increase indicates that this is the case from 15 cm to 8.6 mm for this event. If we take $T=10^7$ K as the temperature of the hot plasma, the emission measure of the thermal electrons becomes 5×10^{49} cm^{-3}. The observed size of the post burst increase at 8.6 mm is consistent with the loop structure suggested by Kawabata (1966) and also with loop structure observed by Vaiana *et al.* (1968) at X-ray wavelength.

However, the free-free emission mechanism cannot account for the decrease of flux density towards short wavelength during the early period of the post-burst increase. Hudson and Ohki (1972) have demonstrated that the radio flux density at 1.8 cm during the early period of thermal X-ray emission is higher than the theoretical value calculated from X-ray data on the basis of the 'hot plasma model'. They therefore suggested that gyro-resonance emissions may be the mechanism of emission at this stage. The present observations also reveal gyro-resonance emission at the same stage.

On the other hand, Shimabukuro (1970) suggested thermal emission from a low temperature, optically thick plasma as a source for the post-burst increases from his observations at 3.3 mm. Since the thermal emission from an optically thick plasma has a spectrum proportional to $1/\lambda^2$, emission of this type dominates the free-free emission from an optically thin hot plasma at the shorter wavelength. Therefore the above conclusion does not exclude the possibility that the post-burst increases at 3.3 mm are mainly due to thermal emissions from a low temperature, optically thick plasma.

Appendix: Thick Target X-Ray Production

Suppose an electron having an energy E impinge on the chromosphere. Then the electron penetrates into the chromosphere with a penetration depth of $l=1/N_i\sigma$, where N_i and σ denote the number density of ambient electrons in the chromosphere, both free and bound, and the cross-section of the ionization loss of the energy, respectively. We adopt the simplest form of $\sigma=\sigma_1(E_1/E)^2$, as the cross-section of ionization loss of energy. Then one obtains the penetration depth

$$l=(E_1/E)^2/(N_i\sigma_1). \tag{A-1}$$

We denote the cross-section of the bremsstrahlung of photons with an energy between $h\nu$ and $h\nu+\mathrm{d}(h\nu)$ by $\sigma(h\nu, E)\,\mathrm{d}(h\nu)$. The X-ray intensity in number of photons at the Earth heliocentric distance R due to an electron beam impinging on the chromosphere is given by

$$I(h\nu)=\frac{1}{4\pi R^2}\int \sigma(h\nu, E)\, v N_i l A_c\, \mathrm{d}N'\Omega, \tag{A-2}$$

where v and Ω represent the velocity of the electron and the solid angle in velocity space of the electron beam respectively. Here A denotes the cross section of the electron beam. The suffix c indicates the value at the chromospheric height here after. We adopt the simplest form of

$$\begin{aligned}\sigma(h\nu, E)&=\sigma_{h\nu_1}\left(\frac{E_1}{h\nu}\right)\left(\frac{E_1}{E}\right)\\&=1.58\times 10^{-26}\left(\frac{10\ \mathrm{keV}}{h\nu_{\mathrm{keV}}}\right)\left(\frac{10\ \mathrm{keV}}{E_{\mathrm{keV}}}\right)\mathrm{cm}^2/(\text{photon energy}).\end{aligned} \tag{A-3}$$

for $h\nu\leqslant E$ and $\sigma(h\nu, E)=0$ for $h\nu>E$.

Inserting Equations (1), (A-1), (A-3) and $\Omega=2\pi(1-\cos\psi_c)$ into Equation (A-2), one obtains

$$I(h\nu)=\frac{2\pi(\delta-1)NA_c c(1-\cos\psi_c)}{4\pi R^2}\frac{\sigma_{h\nu_1}}{\sigma_1}\left(\frac{2E_1}{mc^2}\right)^{1/2}\left(\frac{E_1}{h\nu}\right)\times \times\int_{h\nu/E_1}^{E_2/E_1}\left(\frac{E}{E_1}\right)^{-\delta+1.5}\mathrm{d}\left(\frac{E}{E_1}\right). \tag{A-4}$$

In some articles on solar X-rays, an emission measure $N_i NV$ is given as a measure of X-ray intensity. In the thick target model, the volume V of the X-ray emission region depends on the energy of the impinging electron, because the penetration depth depends on the energy of the electron. As is seen in Equation (A-2), the emission measure of the electrons with an energy higher than E_1 is given by

$$\text{E.M.} = \int N_i l A_c \, \mathrm{d}N'$$

$$= 2\pi(\delta - 1) N A_c (1 - \cos\psi_c) \int_1^{E_2/E_1} \frac{1}{\sigma_1} \left(\frac{E}{E_1}\right)^{-\delta+2} \mathrm{d}\left(\frac{E}{E_1}\right), \qquad \text{(A-5)}$$

if we replace the penetration depth l by its average value.

Equations (A-4) and (A-5) give

$$I(h\nu) = \frac{\delta - 3}{\delta - 2.5} \frac{c}{4\pi R^2} \sigma_{h\nu_1} \left(\frac{2E_1}{mc^2}\right)^{1/2} \left(\frac{h\nu}{E_1}\right)^{-\delta+1.5} \times (\text{E.M.}), \qquad \text{(A-6)}$$

after simple manipulations, when $E_1 < h\nu \ll E_2$. Putting $\delta - 1.5 = \alpha$, we obtain

$$I(h\nu) = \frac{\alpha - 1.5}{\alpha - 1} \frac{c}{4\pi R^2} \sigma_{h\nu_1} \left(\frac{2E_1}{mc^2}\right)^{1/2} \left(\frac{h\nu}{E_1}\right)^{-\alpha} \times (\text{E.M.}). \qquad \text{(A-7)}$$

The relation (A-7) between $I(h\nu)$ and E.M. in the thick target model is the same as the similar relation in the thin target model.

Acknowledgements

The authors would like to thank Prof. F. Moriyama, Tokyo Astronomical Observatory, and Prof. H. Tanaka, Research Institute of Atmospherics, for supplying unpublished observational data. They also would like to thank Dr A. H. Nelson for a critical reading of the manuscript. They would like to acknowlegde the assistance of Mr K. Akita in obtaining the observational material and in data handling. A part of the data reduction was carried out on a FACOM 230-60 at the Nagoya University.

References

Academy of Science, U.S.S.R.: 1970, *Soln. Dann.* No. 11.
Anderson, K. A. and Winckler, J. R.: 1962, *J. Geophys. Res.* **67**, 4103.
Bekefi, G.: 1966, *Radiation Process in Plasmas*, John Wiley & Sons, p. 177.
Elwert, G. and Haug, E.: 1970, *Solar Phys.* **15**, 234.
Feix, G.: 1968, *Geophys. Res.* **73**, 6249.
Hudson, H. S. and Ohki, K.: 1962, *Solar Phys.* **23**, 155.
Kane, S. R. and Anderson, K. A.: 1970, *Astrophys. J.* **162**, 1003.
Kawabata, K.: 1966, *Rep. Ionos. Space. Res. Japan* **20**, 118.
Kawabata, K. and Sofue, Y.: 1972, *Publ. Astron. Soc. Japan* **24**, 469.
Shimabukuro, F. I.: 1970, *Solar Phys.* **15**, 424.

Tindo, I. P., Ivanov, V. D., Mandel'stam, S. L., and Shuryghin, A. I.: 1970, *Solar Phys.* **14**, 204.
Tindo, I. P., Ivanov, V. D., Mandel'stam, S. L., and Shuryghin, A. I.: 1972a, *Solar Phys.* **24**, 429.
Tindo, I. P., Ivanov, V. D., Valníček, B., and Lifshits, M. A.: 1972b, *Solar Phys.* **27**, 426.
Vaiana, G. S., Reidy, W. P., Zehnpfennig., T., Speybroeck, L. van, and Giacconi, R.: 1968, *Science* **161**, 564.
Zheleznyakov, V. V.: 1962, *Soviet Astron. AJ* **6**, 3.